Kelvin waves and the decay of quantum superfluid turbulence

Luiza Kondaurova,[1,2] Victor L'vov,[2] Anna Pomyalov,[2] and Itamar Procaccia[2]
[1]*Institute of Thermophysics, Novosibirsk 630090, Russia*
[2]*Department of Chemical Physics, The Weizmann Institute of Science, Rehovot 76100, Israel*
(Received 19 May 2014; revised manuscript received 12 July 2014; published 4 September 2014)

We present a comprehensive statistical study of free decay of the quantized vortex tangle in superfluid ^{4}He at low and ultralow temperatures $0 \leqslant T \leqslant 1.1$ K. Using high-resolution vortex filament simulations with full Biot-Savart vortex dynamics, we show that for ultralow temperatures $T \lesssim 0.5$ K, when the mutual friction parameters $\alpha \simeq \alpha' < 10^{-5}$, the vortex reconnections excite Kelvin waves with wavelengths λ of the order of the intervortex distance ℓ. These excitations cascade down to the resolution scale $\Delta\xi$ which in our simulations is of the order $\Delta\xi \sim \ell/100$. At this scale, the Kelvin waves are numerically damped by a line-smoothing procedure, that is supposed to mimic the dissipation of Kelvin waves by phonon and roton emission at the scale of the vortex core. We show that the Kelvin wave cascade is statistically important: the shortest available Kelvin waves at the end of the cascade determine the mean vortex-line curvature S, giving $S \gtrsim 30/\ell$, and play a major role in the tangle decay at ultralow temperatures below 0.6 K. The found dependence of ℓS on the resolution scale $\Delta\xi$ agrees with the L'vov-Nazarenko energy spectrum of weakly interacting Kelvin waves $E_{\rm LN} \propto k^{-5/3}$ rather than the spectrum $E_{\rm LN} \propto k^{-1}$, suggested by Vinen for turbulence of Kelvin waves with large amplitudes. We also show that already at $T = 0.8$ K, when α and α' are still very low, $\alpha \simeq \alpha' < 10^{-3}$, the Kelvin wave cascade is fully damped, vortex lines are very smooth, $S \simeq 2/\ell$, and the tangle decay is predominantly caused by the mutual friction.

DOI: 10.1103/PhysRevB.90.094501 PACS number(s): 67.25.dk

I. INTRODUCTION

Below the Bose-Einstein condensation temperature $T_\lambda \approx 2.18$ K, liquid ^{4}He becomes a quantum superfluid, demonstrating inviscid behavior [1]. Aside from the lack of viscosity, the vorticity in ^{4}He is constrained to vortex-line singularities of fixed circulation $\kappa = h/M$, where h is Planck's constant and M is the mass of the ^{4}He atom. These vortex lines have a core radius $a_0 \approx 10^{-8}$ cm, compatible with the interatomic distance. In generic turbulent states, these vortex lines appear as a complex tangle and we denote the typical intervortex distance as ℓ.

There is a growing consensus [2–6] that at large scales $R \gg \ell$, superfluid turbulence exhibits statistical properties that are akin to classical turbulence. In particular, energy cascades in classical and superfluid turbulence are similar up to the intervortex scale ℓ where the discreteness of the vorticity becomes important. It is also believed that in the zero-temperature limit, the energy is further transferred down scales by interacting Kelvin waves [7–11] which are helical perturbations of the individual vortex lines [12]. Finally, at the core radius scale the energy is radiated away by phonons and rotons [2,13].

The direct observation of Kelvin waves which are excited by vortex reconnections was recently achieved by visualizing the motion of submicron particles dispersed in superfluid ^{4}He (cf. Ref. [14]). Nevertheless, as far as we are aware, there are as yet no experimental observation of the Kelvin wave cascade in superfluid ^{4}He (cf. Refs. [10,15–17]). Therefore, at present the confirmation of the statistical importance of Kelvin waves in the evolution of superfluid turbulence should be achieved with computer simulations. This is the main goal of this paper.

Computer simulations of quantum vortex tangle dynamics were pioneered in Ref. [18] with much following research (cf. Refs. [6,9,10,17–28], and references therein. Some studies focused on vortex-line evolution starting from particular and simple initial conditions (see, e.g., Ref. [9]), where a vortex ring approaches a rectilinear vortex or Ref. [25] in which four vortex rings collide. In these and similar simulations, Kelvin waves are excited by vortex reconnections and evidence was found for the development of the direct (from large to small scales) cascade of Kelvin waves. Unfortunately, the numerical resolution was not sufficient to distinguish between available theoretical predictions for the energy spectra of Kelvin waves $E(k)$.

There exist three different predictions for this spectrum. The first was proposed by Vinen [3], and is expected to hold when the amplitudes of the Kelvin waves are large (strong Kelvin wave turbulence):

$$E_{\rm v}(k) = E/k. \tag{1a}$$

Two other predictions were offered for the case of weak Kelvin wave turbulence (small amplitude waves). The first was offered by Kozik and Svitunov [8] (KS) under the assumption of the locality of interactions

$$E_{\rm KS}(k) = E/(\ell^{2/5}k^{7/5}). \tag{1b}$$

The second was predicted by L'vov and Nazarenko [11] (LN) who argued that the interaction of Kelvin waves is not local:

$$E_{\rm LN}(k) = E/(\ell^{2/3}k^{5/3}). \tag{1c}$$

Here, $E \sim \int_{1/\ell}^{1/a_0} E(k)dk$ is the energy density of Kelvin waves per unit vortex-line length, normalized by the ^{4}He density, up to dimensionless numerical constants. Equations (1b) and (1c) should describe exactly the same physical situations and definitely are in contradiction, leading to some debate [29–36]. In fact, recent simulations of the Gross-Pitaevskii equation by Krstulovic [37] support the spectrum (1c). In the most recent

vortex filament simulations by Baggaley and Laurie [38], a remarkable agreement with the LN spectrum (1c) was reported, including the dimensionless coefficient $C_{\rm LN}^{\rm num} \approx 0.308$, very close to the analytic prediction of 0.304 (cf Ref. [39]).

While it appears that Eq. (1c) takes preference on Eq. (1b) for weak Kelvin wave turbulence, the crucial next question is whether Kelvin wave turbulence is indeed weak in realistic experimental situations, say in the decay of counterflow turbulence. If Kelvin wave turbulence happens to be strong, then the Vinen spectrum is likely to be observed.

This paper aims to clarify, at least partially, these and related questions with the help of high-resolution numerical simulation of the decay of counterflow turbulence in ^{4}He at low temperatures $T \leqslant 1.1$ K, including the zero-temperature limit. Details of the numerical procedure are described in Sec. II, the results and their discussion are given in Sec. III. In particular, Sec. III A is devoted to the time evolution of the vortex line density and Sec. III B to the reconnection rate in the free decaying tangle. In the analytical Sec. III C we present a relation between the spectrum of Kelvin waves and the root-mean-square (rms) vortex curvature. Section III D presents our numerical results for the evolution of the rms vortex-line curvature. The analytical and numerical results of Secs. III C and III D allow us to estimate in Sec. III E the upper cutoff of the Kelvin wave spectrum. Section III F discusses the details of the tangle decay at different spatial resolutions and reaches the important conclusions that in the zero-temperature limit vortex tangles exhibit a weak Kelvin wave turbulence. A short summary of the results is given in the end of the paper.

II. NUMERICAL PROCEDURE

Our simulations are aimed at studying the decay of a vortex tangle using the vortex filament method [18]. The details of the implementation were described at length in Ref. [21]. The simulations were carried out in the cubic box $H = 0.1$ cm for temperatures $T = 0$, 0.43, 0.55, 0.8, 0.9, and 1.1 K. The evolution of a point $\boldsymbol{s}$ on the vortex line is described by

$$\frac{d\boldsymbol{s}}{dt} = \boldsymbol{V}_{\rm s} + \boldsymbol{V}_{\rm si} - \alpha \boldsymbol{s}' \times \boldsymbol{V}_{\rm si} + \alpha' \boldsymbol{s}' \times [\boldsymbol{s}' \times \boldsymbol{V}_{\rm si}]. \quad (2a)$$

This equation was solved using the Biot-Savart representation of the velocity, defined by the entire vortex tangle

$$\boldsymbol{V}_{\rm si}(\boldsymbol{s}) = \frac{\kappa}{4\pi} \int_{\mathcal{C}} \frac{(\boldsymbol{s}_1 - \boldsymbol{s}) \cdot d\boldsymbol{s}_1}{|\boldsymbol{s}_1 - \boldsymbol{s}|^3} + \boldsymbol{v}_{\rm bc}. \quad (2b)$$

Here, the vortex line is presented in a parametric form $\boldsymbol{s}(\xi,t)$, where ξ is an arclength, $\boldsymbol{s}' = d\boldsymbol{s}/d\xi$ is a local direction of the vortex line, t is the time, and the integral is taken over the entire vortex tangle configuration $\mathcal{C}$. The influence of the boundary conditions is accounted for in $\boldsymbol{v}_{\rm bc}$. $\boldsymbol{V}_{\rm s}$ is the macroscopic superfluid velocity component. In the reference frame comoving with the superfluid component, $V_{\rm s} = 0$.

The mutual friction parameters $\alpha(T)$ and $\alpha'(T)$ are presented in Table I. For $T = 0.8$, 0.9, and 1.1 K they are taken from Refs. [40,41] by extrapolating the data for B and B' from Figs. 1 and 2 in Ref. [40] and using the relations between B, B' and α, α' and the data for $\rho_{\rm n}$ and ρ from Ref. [41]. For lower temperatures, we used an approximate equation from

TABLE I. Parameters of mutual friction at different temperatures, used in numerical simulations.

T (K)	0	0.43	0.55	0.8	0.9	1.1
$\alpha \times 10^3$	0	0.001	0.01	0.649	2.3	11.2
$\alpha' \times 10^3$	0	0.001	0.01	0.4635	1.4	5.6

Ref. [42]

$$\alpha \simeq \frac{25.3}{\sqrt{T}} \exp\left(-\frac{8.5}{T}\right) + 5.78\,(0.1\,T)^5\,, \quad (3)$$

in which T is in Kelvin. The first term, dominating for $T > 0.5$ K, originates from the roton scattering, discussed in details by Samuels and Donnelly [43]; the second one, taken from Iordanskii's paper [44], describes the contribution of the phonon scattering. Without a corresponding equation for α' in the available literature we took for $T = 0.43$ and 0.55 K $\alpha = \alpha'$ according to the trend at the higher-temperature data (see Table I). Some researches used to neglect the effect of α' at low temperatures, arguing that $\alpha' \ll 1$. Indeed, α' is small, e.g., $\alpha' \approx 0.5 \times 10^{-3}$ at $T = 0.8$ K. Nevertheless, as we show in Appendix, even very small α' (but comparable with α) affects the dynamics of the vortex tangle quite strongly.

In our simulations, periodic conditions were used in all directions. In vortex filament simulations, the reconnections between vortex lines are introduced artificially. The influence of three different popular reconnection criteria [45–47] on the results of such simulations were studied in details in [21]. The first criterion requires only that the two filament points come closer than a predefined distance to trigger reconnections. The second criterion requires reduction of the line length in addition to the geometric proximity. The last criterion is the most strict one and requires that the reconnecting line segments cross in space during the next time step. It was shown that two criteria [46,47] give similar results for all the calculated properties of the vortex tangle, while the criterion [45] gave rise to a very large number of reconnections and large number of small loops that have to be removed algorithmically to ensure stability of the simulations. For simulations of the tangle decay at very low temperature, the role of reconnections becomes very important. Therefore, we have chosen the most efficient numerical reconnection procedure that gives a reliable reconnection rate, the criterion [46]. The reconnection was performed when two line points become closer than the initial line resolution distance $\Delta\xi_{\rm init}$ (that was chosen to be $\Delta\xi_{\rm init} = 5 \times 10^{-4}$ cm), provided the total line length is reduced upon reconnection. The sensitivity of the results to the resolution was clarified by simulating with smaller and larger values of $\Delta\xi_{\rm init}$ as discussed in the following. Points along the vortex line were removed or added during evolution to keep the resolution $\Delta\xi$ inside the interval $\Delta\xi_{\rm init}/1.5 \leqslant \Delta\xi \leqslant 1.5\Delta\xi_{\rm init}$.

This smoothing procedure is required to ensure the accuracy of the calculation of the Biot-Savart integral besides serving as a numerical filter for the high-frequency oscillations of the vortex line, corresponding to the short Kelvin waves with the wavelength $\lambda_{\rm min}$ about $2\Delta\xi$. Removal of the short Kelvin waves serves as their effective damping mechanism at the smallest scale edge of the *direct* energy cascade achieved

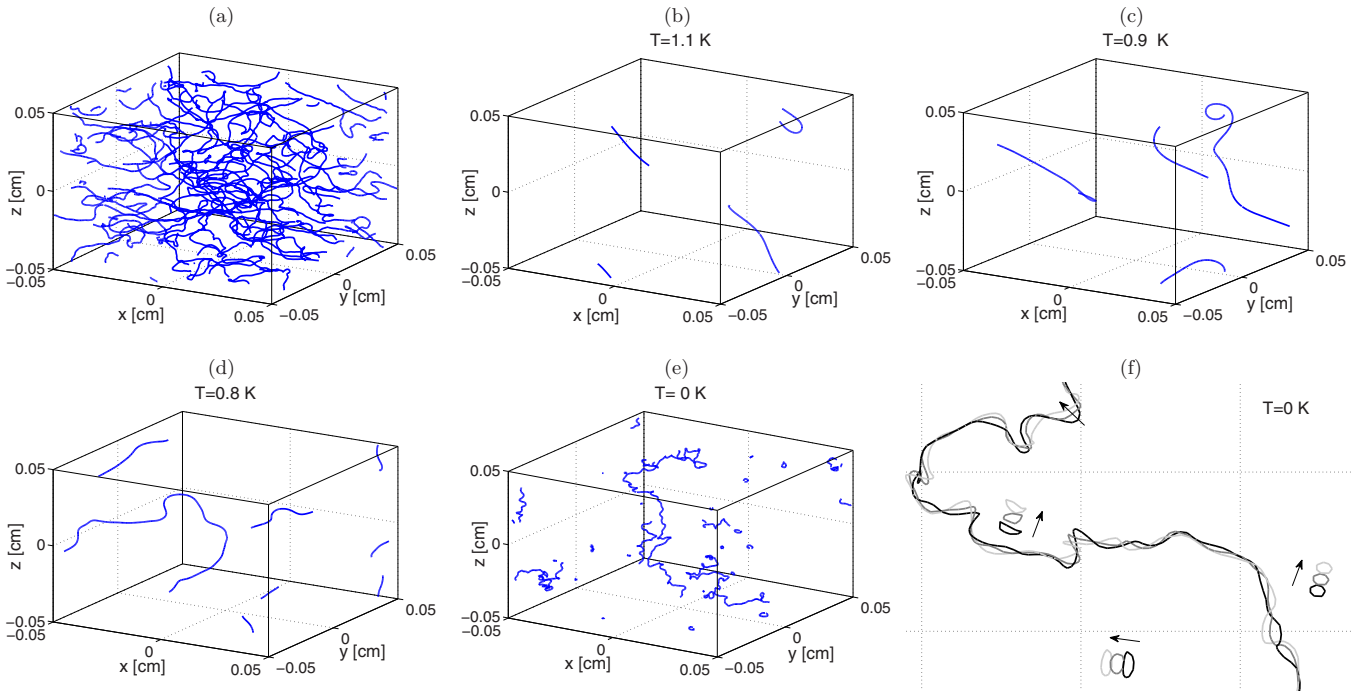

FIG. 1. (Color online) (a) An example of the initial configuration $t = 0$ s, used in the simulations at all the temperatures shown in panels (b)–(f). (b)–(e) Configurations obtained at $t = 50$ s at different temperatures. (f) The fragment of the tangle configuration, shown in panel (e) ($T = 0$) at three successive times separated by 5×10^{-4} s. The black lines correspond to the earliest time $t = 50$ s, the light gray to the latest time. The arrows indicate the direction of the line movement.

in the numerical simulations $\lambda_{\min} \simeq 2\Delta\xi$. We think that this numerical cutoff in the wave-number space does not affect the actual direct cascade in the inertial interval of wavelengths $\lambda \gg \lambda_{\min}$ and therefore leads to the same energy spectrum as an actual dissipation of Kelvin waves at the vortex core radius by radiation of phonons and rotons [2,13].

A possible worry may be based on the existence of the *inverse* (from small to large wavelengthes) cascade of the action of Kelvin waves $n(k)$ [48], related to their energy density $E(k)$ and frequency $\omega(k)$ as follows: $n(k) = E(k)/\omega(k)$.[1] The inverse cascade may potentially affect scales $\lambda \gg \lambda_{\min}$. However, in our case there is no source of Kelvin wave action $n(k)$ at $\lambda \simeq \lambda_{\min}$, only their dissipation, and thus the inverse cascade is not excited. We also remove small loops and loop fragments with three or less line segments. This serves as an additional dissipation mechanism at wavelengths $\lambda \simeq \lambda_{\min}$.

We use the fourth-order Runge Kutta method for the time marching with the time step $\Delta t = 5.6 \times 10^{-5}$ s. Initial conditions were prepared by running steady-state counterflow simulations at $T = 1.9$ K. Taking 32 different realizations in this run we constructed an ensemble consisting of 32 well-developed vortex tangle configurations with a similar vortex-line density (VLD) of about $\mathcal{L}_0 = \mathcal{L}(t = 0) \simeq 6 \times 10^3$ cm^{-2}. Here, the VLD $\mathcal{L}_j(t) = L_j/\Omega$ of a given vortex tangle (indexed by j) is defined as usual [18] via its total length

$$L_j = \int_{\mathcal{C}_j} d\xi, \tag{4}$$

and the sample volume Ω. The integral (4) is performed over the vortex configuration $\mathcal{C}_j$ in the j tangle, i.e., along all vortices. For any object Ψ_j, found on the particular j configuration $\mathcal{C}_j$, we define the ensemble average in the usual way:

$$\langle \Psi \rangle \equiv \frac{1}{N} \sum_{j=1}^{N} \Psi_j. \tag{5}$$

An example of an initial vortex configuration is shown in Fig. 1(a). With the chosen initial vortex-line density, the mean initial intervortex distance $\ell_0 \equiv 1/\sqrt{\langle \mathcal{L}_0 \rangle} \approx 0.013$ cm, which is about 26 times larger than the mean space resolution $\langle \Delta\xi \rangle \approx 5 \times 10^{-4}$ cm.

For this relatively low initial vortex-line density, it was sufficient to account (in the calculation of the Biot-Savart integral) for the tangle configuration within the main computational domain only. More details on this technical issue can be found in Ref. [21].

The initial vortex configurations were allowed to decay according to Eq. (2a) with the parameters α and α' corresponding to different temperatures (see Table I). The simulation was terminated either when the vortex-line density dropped to a background level of about $\mathcal{L}_{\rm bg} = 100$ cm^{-2} or when a predefined decay time for the given temperature has elapsed. The value of $\mathcal{L}_{\rm bg}$ corresponds, e.g., to a configuration with one straight vortex line over the entire computational domain and parallel to its edge. The results for each temperature

[1]The wave action $n(k)$ can be considered as a classical limit of the occupation numbers $N(k)$ in the limit $N(k) \gg 1$: $n(k) \to hN(k)/2\pi$, where h is the Plank constant.

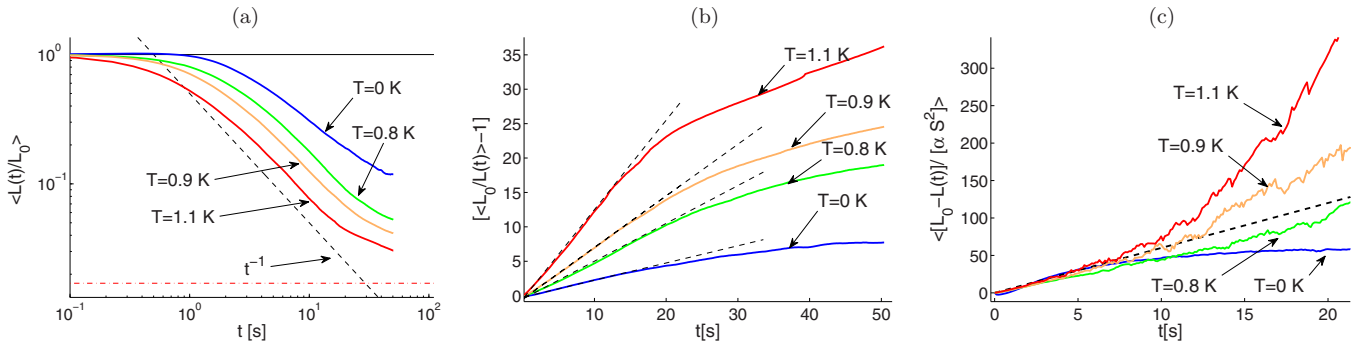

FIG. 2. (Color online) (a) The time dependence of normalized VLD $\langle \mathcal{L}(t)/\mathcal{L}_0 \rangle$, averaged over 32 initial configurations, for $T = 0$ K (blue line), $T = 0.8$ K (green line), $T = 0.9$ K (brown line), and for $T = 1.1$ K (red line). The horizontal dashed-dotted red line shows the background VLD $\mathcal{L}_{bg} = 100$ cm^{-2}. The black dashed line shows the asymptotical decay law $\mathcal{L}(t) \propto t^{-1}$. (b) The evolution of the VLD in the rectifying coordinates (7), $[\langle \mathcal{L}_0/\mathcal{L}(t) \rangle - 1]$ vs t. (c) The evolution of the VLD in another rectifying coordinate $\langle \mathcal{L}_0/\mathcal{L}(t) \rangle$ vs t, dictated by Eqs. (7) and (8): $[\mathcal{L}_0 - \mathcal{L}(t)]/[\alpha \widetilde{S}^2]$.

were obtained by the ensemble averaging over the 32 initial configurations. At the final stage of the simulations, the mean intervortex distance $\ell_{bg} \equiv 1/\sqrt{\mathcal{L}_{bg}} = 0.1$ cm is about 200 times larger than the mean space resolution $\langle \Delta\xi \rangle$.

III. TEMPORAL DECAY OF THE VORTEX TANGLE

The temporal decay of the vortex tangle at $T = 1.9$ K was studied in Ref. [27]. In this paper, we show that new physics emerges at much lower temperatures $T \leqslant 1.1$ K, including the zero-temperature limit. At these temperatures, the entire evolution of the vortex tangle from the initial VLD $\mathcal{L}_0 \simeq 6000$ cm^{-2} to the background level $\mathcal{L}_{bg} \simeq 100$ cm^{-2} takes between 50 to 100 s.

To analyze the physics of the decay of the vortex tangle, it is customary to begin with the traditional VLD dynamics. To provide fuller information, we consider in this section also the time dependence of the rate of reconnection events, and of the curvature of the vortex lines. It turns out that the last quantity is most relevant in the context of the Kelvin waves.

A. Evolution of the vortex-line density and the effective viscosity

The decay of the VLD is usually discussed in the framework of the Vinen equation. Without counterflow velocity [49], it reads as

$$\frac{d\mathcal{L}(t)}{dt} = -\frac{\chi_2 \kappa\, \mathcal{L}^2}{2\pi}, \tag{6}$$

where χ_2 is a phenomenological coefficient. The solution to this equation is

$$\frac{\mathcal{L}_0}{\mathcal{L}(t)} - 1 = \frac{\chi_2}{2\pi}\, \kappa \mathcal{L}_0\, t \equiv b\, t. \tag{7}$$

In Fig. 2, we present the ensemble-averaged results for the evolution of the VLD $\mathcal{L}(t)$ for different temperatures and in different coordinates. Figure 2(a) shows plots of $\ln[\langle \mathcal{L}(t)/\mathcal{L}_0 \rangle]$ with the black dashed line $\mathcal{L} \propto 1/t$, corresponding to the large-t asymptotic of the solution (7). Figure 2(b) shows the same evolution of VLDs, but in rectifying coordinates that are suggested by Eq. (7). One sees that at high temperatures, the decay of the VLD proceeds faster and reaches lower level. For times $t \lesssim 15$ s, these results prove to be consistent with the predictions (7) of the Vinen Eq. (6) for the unbounded vortex tangle with the slope $b \approx 1.2, 0.75, 0.5$, and 0.25 s^{-1} for $T = 1.1, 0.9, 0.8$, and 0 K, respectively. For longer times, when the VLD decay such that the intervortex distance ℓ became compatible with the box size H, this assumption is violated and the numerical results deviate from the prediction (7). It is interesting to note that our numerical results for $T \leqslant 1.1$ K, shown in Fig. 2(b), deviate down from the corresponding straight lines, while for the higher temperature $T = 1.9$ K studied in Ref. [10], they deviate upward.

To clarify the temperature dependence of the decay, consider the phenomenological coefficient χ_2 which is related [18,50] to the mutual friction parameter α and the rms vortex curvature $\widetilde{S}$:[2]

$$\chi_2 = \frac{\alpha\Lambda}{2}\,(\ell\widetilde{S})^2, \tag{8}$$

$$\widetilde{S}^2 \equiv \frac{1}{L}\int_{\mathcal{C}} |\boldsymbol{s}''|^2\, d\xi. \tag{9}$$

Here, $\boldsymbol{s}''(\xi) = d^2\boldsymbol{s}/d\xi^2$ is the local curvature vector of the vortex line. The time evolution of $\widetilde{S}(t)$ at different temperatures will be discussed in Sec. III C.

To check prediction of Eqs. (7) and (8) we rewrote them as follows:

$$\frac{\mathcal{L}_0 - \mathcal{L}(t)}{\alpha \widetilde{S}^2} = \frac{\kappa \mathcal{L}_0}{2\pi}\, t, \tag{10}$$

and plotted in Fig. 2(c) its left-hand side (after ensemble averaging) versus t. The black dashed line has the temperature-independent slope $\kappa\mathcal{L}_0/2\pi$ in Eq. (10). One sees that indeed for $t \lesssim 7$ s all the lines collapse as expected from Eq. (10). Notice that for zero temperature $\alpha = 0$, while for the $T = 0$ K plot (the solid blue line) we choose $\alpha = \alpha_{\rm eff} \simeq 1.2 \times 10^{-4}$, which corresponds to $T \simeq 0.68$ K according to Eq. (3).

Notably, we observe at $T = 0$ K a decay which is similar to the one observed at higher temperatures. Thus, the decay cannot be caused by mutual friction. It is a common belief that

[2]The notation for this object $\widetilde{S}$ is the same as in our Ref. [21] to distinguish it from the mean curvature $\overline{S} = \langle |s''| \rangle$.

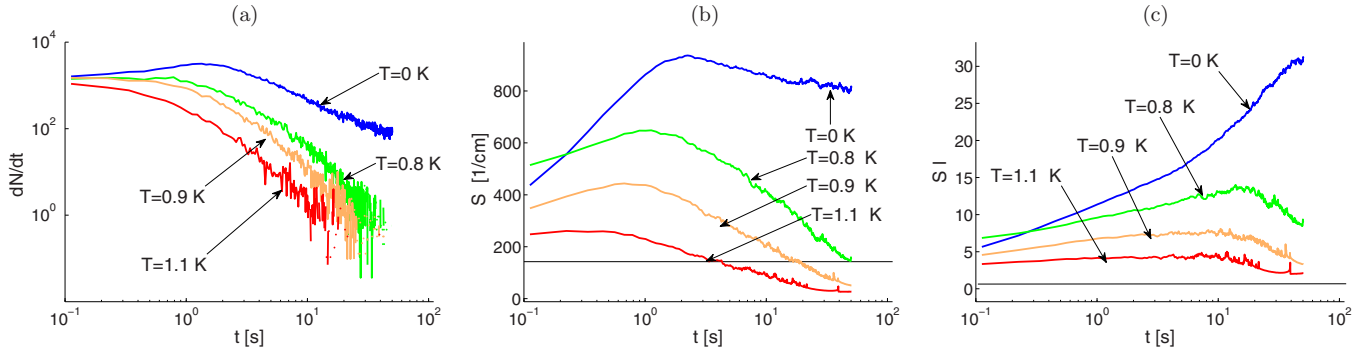

FIG. 3. (Color online) (a) The time dependence of the mean reconnection rate $\langle dN(t)/dt\rangle$ (in s^{-1}) for the same temperatures as in Figs. 1 and 2. (b) The evolution of the rms vortex-line curvature $S(t) \equiv \sqrt{\langle |s''|^2\rangle}$ at different temperatures. (c) The evolution of the dimensionless curvature $\ell(t)S(t)$, normalized by the current intervortex distance $\ell(t)$. Thin horizontal lines show initial curvature [dimensional in (b) and dimensionless in (c)].

the main candidates for the energy dissipation at $T \to 0$ K are the direct Kelvin wave energy cascade and the loop self-crossing that create smaller and smaller loops [7,13,26,51]. Indeed, at the later stage of the tangle evolution, shown in Fig. 1 at $t = 50$ s, there are only smooth vortex lines for $T \geqslant 0.8$ K [Figs. 1(b)–1(d)], while the vortex lines for $T = 0$ K [Fig. 1(e)] are very wrinkled and there are some small loops. A fragment of this configuration, shown in Fig. 1(f) for three successive times, clearly demonstrates the propagation of short Kelvin waves along the vortex line (visible as its meandering around a smooth line) and the fast motion of almost invariant small loops.

Numerical results shown in Fig. 2(b) allow us to estimate the effective (Vinen's) kinematic viscosity $\nu'(T)$ defined via the rate of energy dissipation ε:

$$\varepsilon = \nu'(T)(\kappa\mathcal{L})^2 \simeq \nu'(T)\,\frac{\kappa^2}{\ell^4}. \tag{11}$$

According to Walmsley-Golov [52], the free decay of the VLD depends on ν' as follows:

$$\mathcal{L}(t) = \frac{\Lambda}{4\pi}\,\frac{1}{\nu' t}. \tag{12}$$

Comparing Eqs. (7) and (12), one concludes that the numerical values of b and ν' should be related:

$$b = 4\pi\,\nu'\mathcal{L}_0/\Lambda. \tag{13}$$

Taking our numerical values $\mathcal{L}_0 \approx 6 \times 10^3$ cm^{-2} and $b \approx 1.2\ \mathrm{s}^{-1}$, $0.75\ \mathrm{s}^{-1}$, and $b \approx 0.5\ \mathrm{s}^{-1}$ for $T = 1.2$, 0.9, and 0.8 K, respectively, together with $\Lambda/(4\pi) \approx 1.2$, as in Ref. [52], we estimate the ratio $\nu'/\kappa \approx 0.24$, 0.15, and 0.1 for these temperatures. This estimate is in close agreement with the experimental observations (see Fig. 5 in Ref. [52]). The comparison in the zero-temperature limit requires careful analysis of the effect of finite numerical resolution and will be done elsewhere.

B. Evolution of the reconnection rate

Reconnection events excite Kelvin waves on the vortex lines and in addition may create additional smaller loops by self-crossing. Therefore, an important characteristic of the evolution of the vortex tangle is the reconnection rate defined as the number of reconnection events per unit time $dN(t)/dt$. The computational algorithm includes explicitly the reconnection procedure, thus allowing us to measure this quantity. Figure 3(a) shows that the reconnection rate at $T = 0$ (blue line) is much larger than that at $T = 0.8$ and 0.9 K and $T = 1.1$ K (green, brown, and red lines). This is a combined consequence of two reasons: larger line density [see Fig. 2(a)] and faster motion of the vortex lines caused by their large curvature [see Fig. 2(c)]. The conclusion is that the excitation of Kelvin waves and the production of small loops is ever more efficient when the temperature reduces down to zero.

C. rms of the vortex-line curvature and the energy spectrum of Kelvin waves

For our considerations, the most important information about the level of Kelvin wave excitation is given by the rms of the vortex-line curvature $\widetilde{S}$, defined by Eq. (10). For small deviations of the vortex line δx and δy in the $\boldsymbol{x}$ and $\boldsymbol{y}$ directions from the straight line, oriented along the $\boldsymbol{z}$ axis the vortex length can be approximated as

$$L \approx \int \sqrt{1 + |w'|^2}\,dz\,, \quad w(z) \equiv x + iz\,, \quad w' \equiv \frac{dw}{dz}. \tag{14a}$$

In the same approximation, $|w| \to 0$, $d\xi \approx dz$, and $|s''| \approx |w''| \equiv |d^2w/dz^2|$. This allows one to approximate $\widetilde{S}$ for small amplitudes of Kelvin waves as follows:

$$(\widetilde{S})^2 \approx \frac{1}{L}\int |w''|^2\,dz. \tag{14b}$$

In the local induction approximation, the energy density (per unit mass) of the unit length of the vortex line is $\kappa^2\Lambda/(2\pi)$, where $\Lambda = \ln(\ell/a_0)$ (see, e.g., [7]). Now, expanding the square root in Eq. (14b), we obtain the equation for total energy density (per unit length, per unit mass) of the Kelvin waves:

$$E \approx \frac{\kappa^2\Lambda}{4\pi\,L}\int |w'|^2\,dz. \tag{15a}$$

This allows us to rewrite identically Eq. (14b) as follows:

$$(\widetilde{S})^2 \approx \frac{4\pi}{\kappa^2\Lambda}\,E\,R\,, \quad R \equiv \frac{\int |w''|^2\,dz}{\int |w'|^2\,dz}. \tag{15b}$$

The next step is to rewrite the integrals in the ratio R in the k representation

$$R = \frac{\int k^4 |w_k|^2 dk}{\int k^2 |w_k|^2 dk}, \tag{15c}$$

where w_k is the Fourier image of $w(z)$. Bearing in mind that the canonical amplitudes of Kelvin waves a_k are proportional to w_k and that the Kelvin wave spectrum $E(k) \propto k^2 |a_k|^2$ we present the ratio (15c) as

$$R = \frac{\int k^2 E(k) dk}{\int E(k) dk} = \frac{1}{E} \int k^2 E(k) dk. \tag{15d}$$

Substituting Eq. (15d) into the first of Eq. (15b) we finally get the estimate of $(\widetilde{S})^2$ in terms of the energy spectrum of the Kelvin waves:

$$(\widetilde{S})^2 \simeq \frac{4\pi}{\Lambda \kappa^2} \int_{k_{\min}}^{k_{\max}} k^2 E(k)\, dk. \tag{16}$$

Using the spectrum (1c), which is presumably valid in some interval of scales from the lower wave vector $k_{\min}$ (which is about inverse box size) up to some large-cutoff wave vector $k_{\max}$ (about the inverse core size in the physical system or the resolution scale in the simulations, see below) we get for the case of LN spectrum (1c) of weak turbulence of Kelvin waves:

$$\ell \widetilde{S} \simeq \Phi\, (\ell\, k_{\max})^{2/3}, \tag{17a}$$

where

$$\Phi \equiv \sqrt{4\pi E/(\Lambda \kappa^2)}, \quad E = \int_{k_{\min}}^{k_{\max}} E(k)\, dk. \tag{17b}$$

The same derivation with the KS spectrum (1b) of weak turbulence of Kelvin waves gives

$$\ell \widetilde{S} \simeq \Phi\, (\ell\, k_{\max})^{4/5}, \tag{17c}$$

while in the case of strong turbulence with the Vinen's spectrum (1a) we have

$$\ell \widetilde{S} \simeq \Phi\, (\ell\, k_{\max}). \tag{17d}$$

Note that in any case, the normalized curvature $\ell \widetilde{S}$ is a small-scale effect and no saturation of $\ell \widetilde{S}$ is expected with increasing the line resolution. Notice also that two parameters determine $(\widetilde{S})^2$: the total energy of Kelvin wave excitations, entering Eq. (17a) via the dimensionless parameter Φ, and the dimensionless upper cutoff $\ell k_{\max}$ of the powerlike Kelvin wave energy spectrum. Indeed, without Kelvin waves propagating along the straight vortex lines, the curvature should vanish, i.e., $(\widetilde{S})^2 = 0$. In addition, it is reasonable that the curvature of the vortex line should be dominated by the shortest Kelvin wave in the system, i.e., by $k_{\max}$, the parameter that appears in the estimate (17a) due to the divergence of the integral.

D. Evolution of the mean vortex-line curvature

Armed with the estimate (17a), we can consider now the numerical results for $\widetilde{S}(t)$ at different temperatures, shown in Fig. 3(b), and for $\ell(t)\widetilde{S}(t)$ in Fig. 3(c). In these plots, the initial values $\widetilde{S}(0)$ and $\ell(0)\widetilde{S}(0)$, taken from the stationary vortex configuration at $T = 1.9$ K, are shown by a horizontal solid thin black line. During the first second, when the VLD is practically constant, $\mathcal{L}(t) \simeq \mathcal{L}(0)$ [see Fig. 2(a)], the curvature for $T = 1.1$ K roughly doubles [red line in Fig. 2(c)] and roughly triples for $T = 0.9$ K. The effect is even larger for $T = 0.8$ K. The largest increase of $\widetilde{S}(t)$ corresponds to zero temperature, shown by the blue line in Fig. 2(c). We relate this effect to the increasing level of excitations of Kelvin waves at lower temperatures, partially due to the increase of the reconnection rate, as shown in Fig. 2(b), and partially due to the decrease of Kelvin wave damping due to the mutual friction (see Table I).

During further evolution of the vortex tangles for $t > 1$ s, the curvature $\widetilde{S}(t)$ of the tangles at finite temperatures $T > 0$ K decays, demonstrating a decrease of the Kelvin waves energy, caused by the decrease of the reconnection rate [see Fig. 2(b)], which is responsible for the Kelvin wave excitations. Nevertheless, the product $\ell(t)\widetilde{S}(t)$, as Fig. 2(d) shows, continues to grow during the first 10 s because of the fast growth of $\ell = 1/\sqrt{\mathcal{L}}$. Finally, at later times, $t \sim 10$ s, the curvature $\widetilde{S}(t)$ for $T > 0$ K decays even below its initial value and $\ell(t)\widetilde{S}(t)$ decays to about its initial value $\ell(0)\widetilde{S}(0)$. Accordingly, the configurations Figs. 1(b)–1(d) consist of very smooth vortex lines. The vortex tangles show a completely different behavior at $T = 0$, when there is no mutual friction: the tangles decay is much slower Fig. 1(a)], the reconnection rate is much larger [Fig. 1(b)]. The main difference between zero-temperature and $T > 0$ K cases are the large curvature of the vortex lines that saturates at level $\ell \widetilde{S} \simeq 30$, exceeding substantially the initial level $\ell_0 \widetilde{S}_0 \simeq 2$.

The results for $T = 0.43$ and 0.55 K (not shown in the figures) are very close to those for $T = 0$ K.

E. Estimating the upper cutoff of the Kelvin wave spectrum

With the numerically found value $\ell \widetilde{S} \simeq 30$ for $T = 0$ K, we can estimate the upper cutoff $k_{\max}$ of the Kelvin wave spectrum, using Eq. (17a). Without large-scale motion, the total energy density (per unit length) of the tangle is given as $E = \kappa^2 \Lambda / 4\pi$ (see, e.g., Ref. [29]). The data shown in Fig. 1 allow a rough estimate of the length of straightened vortex lines (i.e., without Kelvin waves) as a half of the total (curved, i.e., with Kelvin waves) vortex lines. This gives $E \simeq E/2 \simeq \Lambda \kappa^2/(4\pi)$. Thus, $\Phi \simeq 1$ in Eq. (17a) and, consequently, $\ell\, k_{\max} \simeq (\ell \widetilde{S})^{3/2} \simeq 160\ \mathrm{cm}^{-1}$ [for the LN spectrum (1c)].

Obviously, the shortest wavelength $\lambda_{\min}$ resolvable in our simulation is about $2\Delta\xi$. Thus, the highest resolvable wave vector is $k_{\mathrm{res}} \simeq \pi/\Delta\xi \simeq 260\ \mathrm{cm}^{-1}$. The consequence is that the spectrum of Kelvin waves cascaded practically all the way down to the numerical resolution. This understanding calls for a careful check of the dependence of the curvature at $T = 0$ on the spatial resolution of the simulation. This is dealt with in the next subsection, resulting in a demonstration that (i) the Kelvin waves are statistically important and (ii) the Kelvin wave dynamics is indeed weakly turbulent.

F. Vortex tangles demonstrate weak Kelvin wave turbulence

The previous section ended with the observation that at $T = 0$ K, the Kelvin wave cascade indeed propagates almost up to the upper end of the available k interval, while for $T \geqslant 0.8$ K

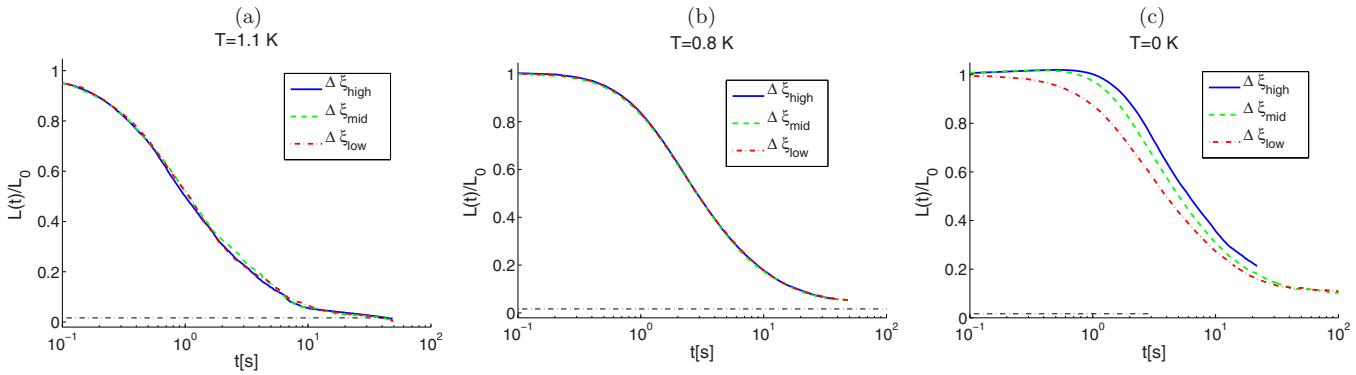

FIG. 4. (Color online) (a)–(c) Comparison of the time dependence of the normalized mean VLD $\langle \mathcal{L}(t)/\mathcal{L}_0 \rangle$ for different resolutions and for $T = 1.1$ and 0.8 K and $T = 0$. The horizontal dashed-dotted red line shows the background VLD $\mathcal{L}_{\rm bg} = 100\ {\rm cm}^{-2}$.

the cascade is only barely visible. This means that even very small mutual friction with $\alpha \lesssim 10^{-3}$ effectively suppresses the cascade. This conclusion is in agreement with the analytical analysis in Ref. [53] according to which for $\alpha \lesssim 10^{-2}$ the Kelvin wave cascade is fully damped.

In our simulations, the line-smoothing procedure at the scale resolution serves as an effective mechanism for damping the Kelvin waves. Therefore, it is important to know how our results depend on the space resolution. For this goal, we plot in Figs. 4(a)–4(c) the evolution of $\langle \mathcal{L}(t)/\mathcal{L}_0 \rangle$ for $T = 1.1$, 0.8, and 0 K with three initial spatial resolutions: $\Delta\xi_{\rm mid} = 5 \times 10^{-4}$ cm, as in all the previous plots (green dashed lines), a higher resolution $\Delta\xi_{\rm high} = 3 \times 10^{-4}$ cm (solid blue lines), and a lower resolution $\Delta\xi_{\rm low} = 8 \times 10^{-4}$ cm (dashed-dotted red lines). We see that for $T = 1.1$ and 0.8 K [Figs. 4(a) and 4(b)], all the three lines practically coincide, as expected: at these temperatures, the Kelvin wave cascade is fully damped at a wavelength $\lambda \sim \ell \gg \Delta\xi$ and therefore the motion at scales about $\Delta\xi$ plays no role. Some minor dependence of the VLD evolution is observed at $T = 0$ K [Fig. 4(c)], when the Kelvin wave cascade does reach the resolution limit. This can be caused by several reasons, related to the finiteness of the scale separation between ℓ and $\Delta\xi$. Their analysis is beyond the scope of this paper.

The evolution of $\ell\widetilde{S}(t)$, shown in Figs. 5(a)–5(c) for the same set of parameters, is much more sensitive to the resolution. This is expected because the curvature is determined by the shortest Kelvin waves in the system. Correspondingly, at the higher temperature $T = 1.1$ K [Fig. 5(a)], where the Kelvin waves are excited only with $\lambda \simeq \ell$, there is practically no dependence on the resolution. For $T = 0.8$ K, when only the tails of the Kelvin wave energy spectrum reaches the resolution scale one sees in Fig. 5(b) some weak dependence on the resolution.

According to our understanding, the Kelvin wave cascade reaches the resolution limit $k_{\rm max} \lesssim k_{\rm res} \simeq \pi/\Delta\xi$, only at ultralow temperatures, below $T = 0.5$ K. This should lead to an essential dependence of $\widetilde{S}\ell$ on the resolution. This is indeed the case, as one sees in Fig. 5(c).

Employing the LN spectrum of weak wave turbulence (17a) at $T = 0$ K we predicted $\ell\widetilde{S} \propto \Delta\xi^{-2/3}$ according to Eq. (1c). Thus, the curvature $\ell\widetilde{S}$ calculated with different line resolutions and compensated by $(\Delta\xi/\Delta\xi_{\rm mid})^{2/3}$ should collapse to a single line. This is indeed the case [cf. Fig. 6(a)] in comparison with the noncompensated curvatures in Fig. 5(c). For completeness, we show in Fig. 6(b) the time dependence of the dimensionless curvature $\ell\widetilde{S}$, compensated by $(\Delta\xi/\Delta\xi_{\rm mid})^{4/5}$, as predicted by Eq. (17c) for the KS spectrum (1b) of weak wave turbulence. According to our understanding, collapse in Fig. 6(a) is slightly better than in Fig. 6(b), at least for later times $t > 3$ s, when a significant decay of the vortex-line density occurs [see Fig. 2(a)]. Nevertheless, the difference between these two cases (LN and KS spectra of weak wave turbulence) is modest and cannot serve as a decisive argument.

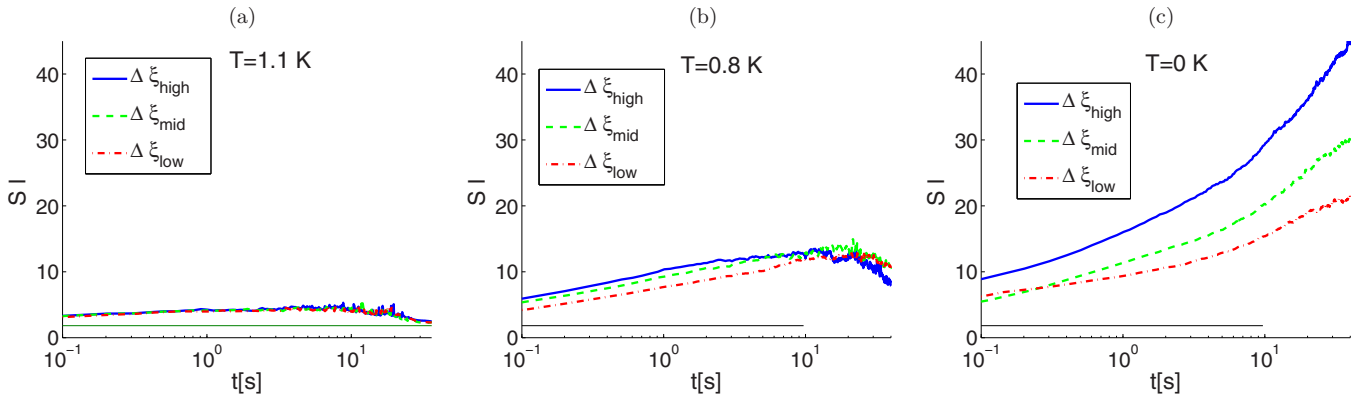

FIG. 5. (Color online) Comparison of the time dependence of the normalized curvature $\ell(t)\widetilde{S}$ for different resolutions and the same temperatures.

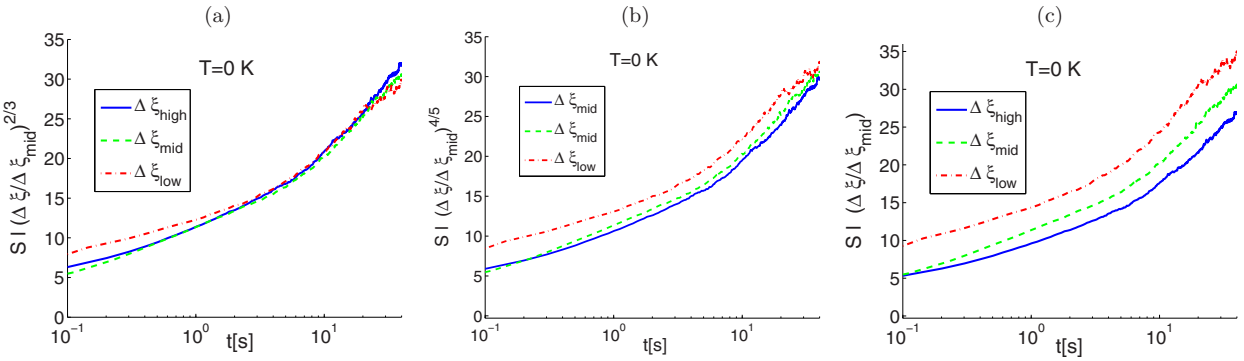

FIG. 6. (Color online) Evolution of the vortex-line curvatures $\ell\widetilde{S}$ at different scale resolutions compensated by $(\Delta\xi/\Delta\xi_{\rm mid})^{2/3}$ (a), by $(\Delta\xi/\Delta\xi_{\rm mid})^{4/5}$ (b), and by $(\Delta\xi/\Delta\xi_{\rm mid})$ (c).

This is not our goal here. As we explained in the Introduction, this can be done by specially designed numerical simulations like those in Refs. [37,38].

At this point, we can pose the important question of the nature of the Kelvin wave turbulence. Is it the weak turbulence characterized by the one of the two spectra (LN or KS) or the strong turbulence with the Vinen spectrum (1a), for which the data should collapse with the linear compensation by $\Delta\xi/\Delta\xi_{\rm mid}$, shown in Fig. 6(c). One sees that the lines do not collapse, in contrast to Fig. 6(a) and 6(b) with the LN and KS compensation. We consider these results as a clear evidence of a weak wave turbulence regime (presumably with the LN spectrum) in the decay of counterflow turbulence at ultralow temperatures.

There exist analytical arguments in favor of weak wave turbulence regime of energy cascade by Kelvin waves. Using LN kinetic equation (5) suggested in Ref. [11], the damping frequency of Kelvin waves can be estimated as

$$\gamma(k) \simeq \frac{\varepsilon^{2/3}}{\kappa} k^{2/3}\ell^{4/3}, \tag{18a}$$

and compared with the Kelvin wave frequency

$$\omega(k) = \frac{\Lambda\kappa}{4\pi}k^2 \simeq \kappa k^2. \tag{18b}$$

The last estimate accounts for that numerically $\Lambda/(4\pi)$ is close to unity. It is known [54] that the applicability criterion of the regime of weak wave turbulence requires $\gamma(k) \ll \omega(k)$. In our case,

$$\zeta(k) \equiv \frac{\gamma(k)}{\omega(k)} \simeq \frac{\varepsilon^{2/3}\,\ell^{4/3}}{\kappa^2\,k^{4/3}}. \tag{19a}$$

With the estimate (11) for the rate of energy dissipation ε via effective Vinen's viscosity ν', Eq. (19a) gives

$$\zeta(k) \simeq \left(\frac{\nu'}{\kappa}\right)^{2/3} \frac{1}{(k\ell)^{4/3}}. \tag{19b}$$

In our simulations and experimentally [52] $\nu' \simeq 0.1\,\kappa$. This means that even at the beginning of the inertial interval, when $k\ell \simeq 1$, $\zeta < 1$ and one should expect a regime which is close to the weak wave turbulence case. As k increases, ζ quickly decreases and becomes much smaller than unity at the short-wavelength edge of the inertial interval, where $k_{\rm max} \simeq 1/(\Delta\xi)$. Here, we expect a pure weak wave turbulence regime, presumably with the LN spectrum.

Notice that during the decay of the vortex tangle, the total width of the inertial interval $\ell/(\Delta\xi)$ increases and therefore the approximation of the weak wave turbulence becomes better. In particular, this explains why the LN collapse in Fig. 6 becomes better at larger times $t > 3$ s.

Notice that the collapse Eqs. (17) assume that the parameter Φ, defined by Eq. (17b), is independent of the resolution $\Delta\xi$. This is a reasonable approximation because the integral in Eq. (17b) is dominated by the lower cutoff of the power spectra $k_{\rm min}$. For example, for the LN spectrum (1c), the $\Phi(\Delta\xi)$ dependence can be estimated as $\Phi(\Delta\xi) \propto [1 - \frac{1}{2}(\Delta\xi/\ell)^{2/3}]$, and consequently can be approximated by a constant with accuracy better than 6% for our numerical parameters even at small times $t < 1$ s. During the time evolution ℓ increases and the accuracy improves further.

We also have to mention that the difference in the cutoff lengths for low and high resolution is only a factor of $\frac{8}{3} \approx 2.7$ and cannot be straightforwardly used (for example by plotting $\ell\widetilde{S}$ versus $\ell k_{\rm max}$) for any kind of argument in favor of power-law scaling. Instead, we have plotted in Fig. 6 the scale compensated plots $\ell\widetilde{S}(\ell k_{\rm max})^x$ versus t and see a clear difference for $x = \frac{2}{3}$, $\frac{4}{5}$, and 1 in Figs. 6(a)–6(c).

Definitely, it would be nice to see some Kelvin wave spectra at low temperatures, for example, analyzing a configuration like the one observed in Fig. 1(e), where a long filament with Kelvin waves is visible. Unfortunately, this is an almost impossible task with our numerical resolutions (with only about 25–30 points on the intervortex scale ℓ), giving less than a decade of inertial interval with Kelvin waves. As we mentioned in the Introduction, it is hardly possible to distinguish between the theoretical predictions (1a), (1b), and (1c), even with the better resolution achievable in studies of vortex-line evolutions from much simpler initial configurations in Refs. [9,25]. This can be done only with specially arranged simulations in which Kelvin waves are excited on a straight line, say with 1024 points, as in Ref. [38].

Our goal in this paper was different: to demonstrate that Kelvin waves play a statistically important role in the decay of a random vortex tangle, generated by counterflow turbulence. Fortunately, analyzing the time evolution of the mean rescaled vortex curvature in Fig. 6 (instead of the direct measurement of the scaling exponents) we were able to distinguish between

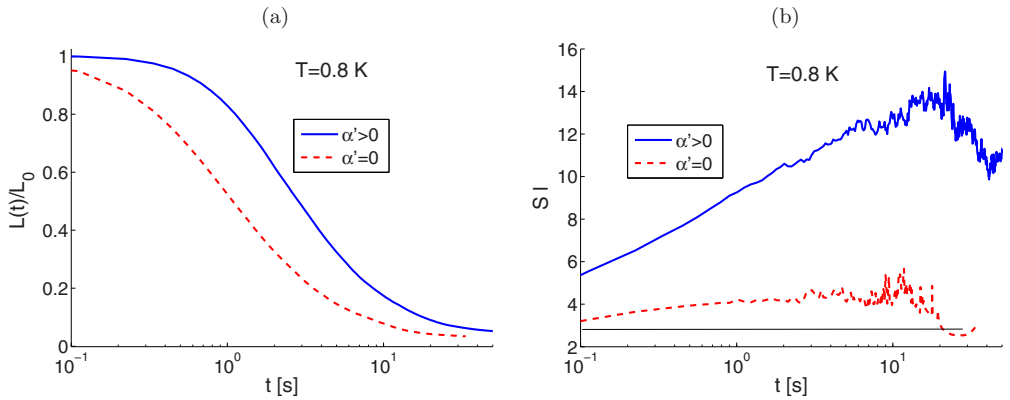

FIG. 7. (Color online) Comparison of the evolution of the normalized VLD $\mathcal{L}(t)/\mathcal{L}(0)$ (a) and of the normalized curvature $S(t)\ell(t)$ (b) for the simulations with $\alpha = 6.49 \times 10^{-4}$ and $\alpha' = 4.635 \times 10^{-4}$ (corresponding to $T = 0.8$ K, see Table I), shown by solid blue lines, and with the same $\alpha = 6.49 \times 10^{-4}$, but $\alpha' = 0$ (dashed red lines).

strong and weak wave turbulence spectra of Kelvin waves. In some sense, this approach is an analog of the extended self-similarity analysis by Benzi *et al.* [55], successfully used in the past for the scaling analysis of the experimental and numerical data in developed classical turbulence.

IV. SUMMARY

We reported a comprehensive numerical study of the statistical properties of the free decaying vortex tangle at low and ultralow temperatures. The simulations were carried out in the framework of the full Biot-Savart equations using vortex filament method with high spatial resolution $\Delta\xi$ which encompasses two decades of the Kelvin wave cascade below the intervortex scale ℓ.

We estimated from our numerical results the effective Vinen's viscosity and demonstrated its good agreement with the experimental results [52] in Manchester spin-down experiment in ^{4}He.

We showed that even very small mutual friction with $\alpha \gtrsim 10^{-4}$ effectively suppresses the Kelvin wave cascade such that there survive only Kelvin waves with the wavelength $\lambda \simeq \ell$. At ultralow temperatures $T \lesssim 0.5$ K, when $\alpha \lesssim 10^{-5}$, the Kelvin wave cascade is developing up to the resolution scale with $\lambda \simeq 2\Delta\xi$, where it is terminated in the simulations by the line-smoothing procedure that mimics the dissipation of Kelvin waves by the emission of phonons and rotons at the vortex-core scale in real flows.

We showed that the Kelvin wave cascade is statistically important: the shortest available Kelvin waves at the end of the cascade determine the mean vortex-line curvature $\widetilde{S}$, giving $\widetilde{S} \simeq 30/\ell$. We showed that in the decay of counterflow turbulence there is a regime of weak turbulence of Kelvin waves with the LN spectrum (1c) rather than the strong turbulence regime with the Vinen spectrum (1a).

ACKNOWLEDGMENTS

We acknowledge useful comments by A. Golov and all the three anonymous referees. This paper had been supported in part by the Minerva Foundation, Munich, Germany, and by Grant No. 14-29-00093 from Russian Science Foundation. L.K. acknowledges the kind hospitality at the Weizmann Institute of Science during the main part of the project.

APPENDIX: IMPORTANCE OF THE ENERGY-CONSERVING MUTUAL FRICTION FORCE

As we discussed in Sec. II, the experimental data for the mutual friction parameters are not available for temperatures below 1 K. Parameter α can be estimated analytically by Eq. (3). Corresponding equations for α' are not available. One may think that very small α', responsible for nondissipative interactions, is not important and can be neglected. To check this idea, we compare in Fig. 7 numerical results for the VLD and curvature evolution of the tangle with $\alpha = 6.49 \times 10^{-4}$ and $\alpha' = 4.635 \times 10^{-4}$, corresponding to $T = 0.8$ K, with the evolution with the same α, but $\alpha' = 0$. One sees that the results differ essentially and conclude that even very small α' cannot be neglected. This can be related to the geometry of the vortex lines approaching the reconnection, that effect the reconnection rate.

[1] A. F. Annett, *Superconductivity, Superfluids and Condensates* (Oxford University Press, Oxford, 2004).
[2] W. F. Vinen, Phys. Rev. B **61**, 1410 (2000).
[3] W. F. Vinen and J. J. Niemela, J. Low Temp. Phys. **128**, 167 (2002).
[4] W. F. Vinen, J. Low Temp. Phys. **161**, 419 (2010).
[5] P.-E. Roche, C. F. Barenghi, and E. Leveque, Europhys. Lett. **87**, 54006 (2009).
[6] C. F. Barenghi, V. S. L'vov, and P. E. Roche, Proc. Natl. Acad. Sci. USA **111**, 4683 (2014).
[7] B. V. Svistunov, Phys. Rev. B **52**, 3647 (1995).

[8] E. Kozik and B. Svistunov, Phys. Rev. Lett. **92**, 035301 (2004); **94**, 025301 (2005).
[9] T. Araki and M. Tsubota, J. Low Temp. Phys. **121**, 405 (2000).
[10] W. F. Vinen, M. Tsubota, and A. Mitani, Phys. Rev. Lett. **91**, 135301 (2003).
[11] V. S. L'vov and S. Nazarenko, Pis'ma Zh. Eksp. Teor. Fiz. **91**, 464 (2010) [JETP Lett. **91**, 428 (2010)].
[12] W. Thomson (Lord Kelvin), Philos. Mag. **10**, 155 (1880).
[13] W. F. Vinen, Phys. Rev. B **64**, 134520 (2001).
[14] E. Fonda, D. P. Meichle, N. T. Ouellette, S. Hormoz, and D. P. Lathrop, Proc. Natl. Acad. Sci. USA **111**, 4707 (2014).
[15] V. B. Eltsov, A. I. Golov, R. de Graaf, R. Hanninen, M. Krusius, V. S. Lvov, and R. E. Solntsev, Phys. Rev. Lett. **99**, 265301 (2007).
[16] L. Skrbek and K. R. Sreenivasan, Phys. Fluids **24**, 011301 (2012).
[17] C. F. Barenghi, L. Skrbek, and K. R. Sreenivasan, Proc. Natl. Acad. Sci. USA **111**, 4647 (2014).
[18] K. W. Schwarz, Phys. Rev. B **38**, 2398 (1988).
[19] R. Hänninen, Phys. Rev. B **88**, 054511 (2013).
[20] R. Hänninen and A. W. Baggaley, Proc. Natl. Acad. Sci. USA **111**, 4667 (2014).
[21] L. Kondaurova, V. L'vov, A. Pomyalov, and I. Procaccia, Phys. Rev. B **89**, 014502 (2014).
[22] E. Kozik and B. Svistunov, Phys. Rev. B **72**, 172505 (2005).
[23] T. Araki, M. Tsubota, and S. K. Nemirovskii, Phys. Rev. Lett. **89**, 145301 (2002).
[24] S. K. Nemirovskii, J. Pakleza, and W. Poppe, Russ. J. Eng. Thermophys. **3**, 369 (1993).
[25] D. Kivotides, J. C. Vassilicos, D. C. Samuels, and C. F. Barenghi, Phys. Rev. Lett. **86**, 3080 (2001).
[26] M. Tsubota, T. Araki, and S. K. Nemirovskii, Phys. Rev. B **62**, 11751 (2000).
[27] Y. Mineda, M. Tsubota, and W. F. Vinen, J. Low Temp. Phys. **171**, 511 (2013).
[28] L. P. Kondaurova and S. K. Nemirovskii, Phys. Rev. B **86**, 134506 (2012).
[29] J. Laurie, V. S. L'vov, S. Nazarenko, and O. Rudenko, Phys. Rev. B **81**, 104526 (2010).
[30] V. V. Lebedev and V. S. L'vov, J. Low Temp. Phys. **161**, 548 (2010).
[31] V. V. Lebedev, V. S. L'vov, and S. V. Nazarenko, J. Low Temp. Phys. **161**, 606 (2010).
[32] E. Kozik and B. V. Svistunov, Phys. Rev. B **82**, 140510 (2010).
[33] E. B. Sonin, Phys. Rev. B **85**, 104516 (2012).
[34] V. S. L'vov and S. V. Nazarenko, Phys. Rev. B **86**, 226501 (2012).
[35] E. B. Sonin, Phys. Rev. B **86**, 226502 (2012).
[36] A. W. Baggaley and C. F. Barenghi, Phys. Rev. B **83**, 134509 (2011).
[37] G. Krstulovic, Phys. Rev. E **86**, 055301 (2012).
[38] A. W. Baggaley and J. Laurie, Phys. Rev. B **89**, 014504 (2014).
[39] L. Boué, R. Dasgupta, J. Laurie, V. S. L'vov, S. Nazarenko, and I. Procaccia, Phys. Rev. B **84**, 064516 (2011).
[40] C. F. Barenghi, R. J. Donnelly, and W. F. Vinen, J. Low Temp. Phys. **52**, 189 (1983).
[41] R. J. Donnelly and C. F. Barenghi, J. Phys. Chem. Ref. Data **27**, 1217 (1998).
[42] V. B. Eltsov, R. De Graaf, P. J. Heikkinen, M. Krusius, R. E. Solntsev, V. S. L'vov, A. I. Golov, and P. M. Walmsley, Prog. Low Temp. Phys. **16**, 45 (2009).
[43] D. C. Samuels and R. J. Donnelly, Phys. Rev. Lett. **65**, 187 (1990).
[44] S. V. Iordanskii, Zh. Eksp. Teor. Fiz. **49**, 225 (1965) [Sov. Phys.–JETP **22**, 160 (1966)].
[45] H. Adachi, S. Fujiyama, and M. Tsubota, Phys. Rev. B **81**, 104511 (2010).
[46] David C. Samuels, Phys. Rev. B **46**, 11714 (1992).
[47] L. P. Kondaurova, V. A. Andryuschenko, and S. K. Nemirovskii, J. Low Temp. Phys. **150**, 415 (2008).
[48] S. Nazarenko, JETP Lett. **83**, 198 (2006).
[49] W. F. Vinen, Proc. R. Soc. London, Ser. A **240**, 114 (1957); **242**, 493 (1957).
[50] L. Skrbek, A. V. Gordeev, and F. Soukup, Phys. Rev. E **67**, 047302 (2003).
[51] M. B. Kursa, K. Bajer, and T. Lipniacki, Phys. Rev. B **83**, 014515 (2011).
[52] P. W. Walmsley and A. I. Golov, Phys. Rev. Lett. **100**, 245301 (2008).
[53] L. Boué, V. S. L'vov, and I. Procaccia, Europhys. Lett. **99**, 46003 (2012).
[54] V. E. Zakharov, V. S. L'vov, and G. E. Falkovich, *Kolmogorov Spectra of Turbulence* (Springer, Berlin 1992).
[55] R. Benzi, S. Ciliberto, R. Tripiccione, C. Baudet, F. Massaioli, and S. Succi, Phys. Rev. E **48**, R29 (1993).